PHYSICAL REVIEW B **93**, 134419 (2016)

Spin reorientation transition of magnetite (001)

Laura Martín-García,[1] Arantzazu Mascaraque,[2,3] Beatriz M. Pabón,[2,3] Roland Bliem,[4] Gareth S. Parkinson,[4] Gong Chen (陈宫),[5] Andreas K. Schmid,[5] and Juan de la Figuera[1,*]

[1]*Instituto de Química Física "Rocasolano," CSIC, Madrid E-28006, Spain*
[2]*Dpto. de Física de Materiales, Universidad Complutense de Madrid E-28040, Spain*
[3]*Unidad Asociada IQFR(CSIC)-UCM, Madrid E-28040, Spain*
[4]*Institute of Applied Physics, Vienna University of Technology, Vienna A-1040, Austria*
[5]*NCEM, Molecular Foundry, Lawrence Berkeley National Laboratory, Berkeley, California 94720, USA*

(Received 15 January 2016; revised manuscript received 18 March 2016; published 18 April 2016)

We have imaged the rearrangement of the magnetic domains on magnetite (001) when crossing the spin reorientation transition and the Verwey transition with nanometer resolution. By means of spin-polarized low-energy electron microscopy we have monitored the change in the easy axes lowering the temperature through both transitions in remanence. The spin reorientation transition occurs in two steps: initial nucleation and growth of domains with a new surface magnetic orientation is followed by a smooth evolution.

DOI: 10.1103/PhysRevB.93.134419

I. INTRODUCTION

Magnetism in magnetite, aside from its historical interest [1], has presented puzzles that have motivated the advance of solid state physics and magnetism. At room temperature, magnetite has a magnetocrystalline cubic anisotropy that favors easy axes along the ⟨111⟩ directions, and that is smaller than the dipolar anisotropy [2]. Early on, magnetite was found to present a phase transition, the Verwey transition [3], where its resistivity changes by two orders of magnitude. Furthermore, below the Verwey transition temperature T_v magnetite adopts a monoclinic structure and becomes ferroelectric and ferroelastic.

The evolution of the magnetocrystalline anisotropy of magnetite in the cubic phase is quite striking [4–7]. The first-order magnetocrystalline anisotropy K_1 changes sign at the spin reorientation transition T_{srt}, typically at a temperature about 10 K above the Verwey transition temperature. The magnetic easy axes change from the room-temperature ⟨111⟩ ones to the ⟨100⟩ axes below T_{srt} [7]. The spin reorientation transition has been detected by the evolution of the saturation magnetization [8], ac magnetic susceptibility [9], ferromagnetic resonance [4], muon spin spectroscopy [10], or nuclear magnetic resonance [11]. The similar trend in the temperatures of both transitions upon doping has been taken as a proof of a common origin [6,9], although this has been disputed [12,13].

There are few temperature-dependent experiments observing the magnetic domains of magnetite in real space. Domains have been observed at the Verwey transition by transmission electron microscopy in micrometer-sized grains [14,15], observations that have helped understand the interaction of magnetic domain walls and structural domains in the monoclinic phase of magnetite. But, to the best of our knowledge, no observations have been reported following the changes in real space through the spin reorientation transition itself. Thus, the detailed micromagnetic evolution through the spin reorientation transition has not been determined. For example, it is not known whether the easy axes change continuously through a second-order transition [13], or abruptly from one set of magnetic easy axes to another. This situation is in contrast to the effort devoted to the characterization of the Verwey transition. The Verwey transition has long been determined to be first order for small deviations of the stoichiometry while it becomes second order for larger deviations and is eventually suppressed [16]. We have performed previous work on magnetite by low-energy electron microscopy [17,18]. Here, we focus on the fate of particular magnetic domains observed when cooling through the spin reorientation and the Verwey transitions.

II. EXPERIMENTAL METHODS

The experiments have been performed in a spin-polarized low-energy electron microscope (SPLEEM [19]). The microscope is equipped with a GaAs spin-polarized electron source coupled to a spin manipulator. The manipulator is used to adjust the spin direction of the electron beam with respect to the sample surface [20–24].

Two magnetite samples with (001) orientation have been studied. The first one is a crystal of natural origin [25]. It has been cut to a hat shape to provide a uniform potential surface in front of the objective lens for use in variable temperature measurements. Its T_v is 114 K. The second one is a highly stoichiometric synthetic crystal with a bulk Verwey temperature of 123 K, with a rectangular shape of 10 mm × 4 mm [17]. This sample provides a reference stoichiometric magnetite [26], but its small size makes it unsuitable for variable temperature experiments due to the difficulty in correcting the normal orientation. The temperature was measured for both samples by means of a Pt1000 resistor. The samples were cleaned after introduction in the SPLEEM system by a few cycles of 10 min of sputtering with Ar ions at 1 keV followed by annealing to 870 K in 10^{-6} Torr of O_2 for tens of minutes.

III. RESULTS AND DISCUSSION

LEEM images show mostly features related to the topography of the crystal surface. An example is shown in Fig. 1(a). The image corresponds to the natural crystal after tens of cleaning cycles. The distinctive topography has square

*juan.delafiguera@iqfr.csic.es

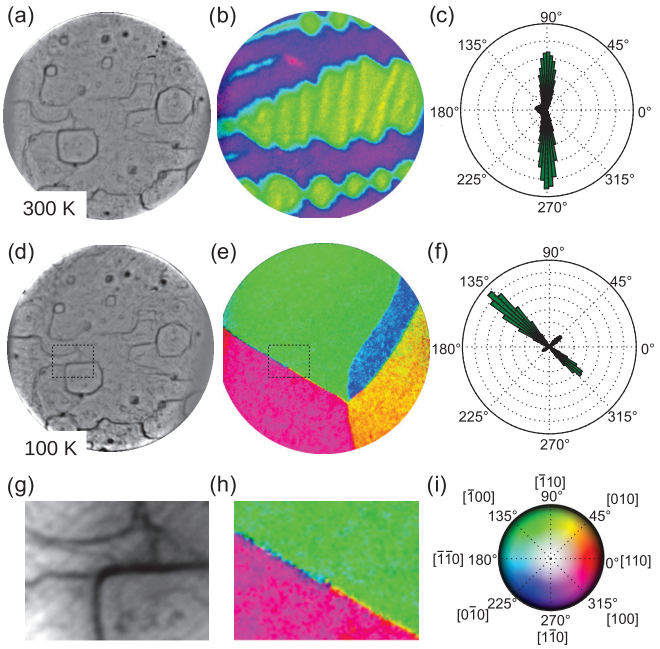

FIG. 1. (a) LEEM image of the surface of $Fe_3O_4(001)$ at room temperature (300 K). The field of view is 12 μm and the start voltage is 8 V. (b) Composite color image indicating the local magnetization vector using the color wheel shown in (i). (c) Polar histogram of the magnetization form the data shown in (b). (d) LEEM image of the same area after cooling down to 100 K. (e) Composite color image of the magnetization. (f) Polar histogram. (g) Detail of the area marked in (d) with a dashed box, 2.9 μm wide. (h) Magnetic contrast in the area shown in (g). (i) Color wheel indicating the correspondence between color and direction in images (b), (e) and (h).

"mesas" or mounds covering the surface as well as step bunches characteristic of "aged" (i.e., subject to many cleaning cycles) (001) magnetite samples [27]. The square mesas are aligned with the compact directions of the magnetite surface, i.e., the [110] and [$\bar{1}$10] directions which correspond to the x and y axes of the figure. They develop during the sputtering and annealing cycles due to the surface growth upon oxygen exposure described in Ref. [28].

A fresh surface introduced from air does not show magnetic contrast in SPLEEM. We attribute this to the lack of good order on the surface. Only when the crystal surface has been cleaned by several cycles of sputtering and annealing so it shows the $\sqrt{2} \times \sqrt{2}R45^\circ$ [27] reconstruction, magnetic contrast is observed. The current model of the reconstructed surface, the subsurface cation vacancy model [29], makes specific predictions on the magnetic moment of the near-surface regions, predictions that have been corroborated by x-ray magnetic circular dichroism [30]. In the present experiments, we focus instead on the distribution of magnetic domains. Although these magnetic domains are imaged through the spin reflectivity of the last few atomic layers, their origin arises from a larger region, defined in magnetic terms: the region of the surface where the shape anisotropy is large compared with the magnetocrystalline anisotropy. We believe that in this sense our observations are not affected by the detailed atomic surface structure termination. By combining asymmetry images along orthogonal directions, we can determine the three-dimensional magnetization vector. The image in Fig. 1(b) shows the in-plane distribution of the magnetization on the same area observed in Fig. 1(a), employing a color palette to indicate the vector direction using the color wheel of Fig. 1(i). Magnetic domains are observed to be completely unrelated to the topographic features. The magnetic domains in the image are oriented mostly along the [$\bar{1}$10] axis: the green-yellow domains correspond to [$\bar{1}$10] (90°), while the blue-purple ones correspond to [1$\bar{1}$0] (270°). The domain walls are wavy, and have a [$\bar{1}\bar{1}$0] orientation of the magnetization (180°). No out-of-plane magnetic contrast is detected (not shown). The magnetic domains observed correspond to the surface region, as the contrast originates from exchange scattering with the electron beam at low electron energies [31]. There is a band pattern in the greenish domains, with a typical micron-wide periodicity (observed in the image as green and yellow bands), while the oppositely oriented domains do not present such a structure.

As a complementary way to visualize the magnetization orientation, we present in Fig. 1(c) a polar histogram of the distribution of magnetization values from the image shown in Fig. 1(b). As discussing in the following, this combination of polar histogram and color images provides information crucial to follow the evolution of the surface. At room temperature, they clearly show that in most of the surface the magnetization is oriented along the 90° and the 270° directions. The areas corresponding to the domain walls can also be observed in the histogram, along the 180° direction. We note that the Fe_3O_4 easy axes at room temperature are the ⟨111⟩ ones [7]. As already reported [18], both the in-plane easy axis directions and the curved domain walls likely originate from the competition of the magnetocrystalline anisotropy and the shape anisotropy on the magnetite (001) near-surface region: the observed surface easy axes correspond to the projection of the bulk ones onto the surface plane. We have observed similar patterns in several samples, both synthetic and natural crystals with different stoichiometries [18,30], and at widely differing cleaning stages, so we believe they are an intrinsic feature of the $Fe_3O_4(001)$ surface. We remark that this style of domains is very different from domains experimentally observed in magnetite thin films with (001) orientation [32–35]. The difference in domain size and shape on thin films is likely due to the presence of antiphase domain boundaries (APBs). APBs strongly affect the local magnetization [36], but they are rare in bulk single crystals.

When crossing the Verwey transition, the magnetite crystal structure transforms into a monoclinic one. The high-temperature cubic single crystal becomes a polycrystal with different local monoclinic orientations (i.e., magnetite undergoes a ferroelastic [37] transition). Within a given average monoclinic direction, lamellar twins are observed sharing their $[100]_m$ and $[010]_m$ axes. Transmission electron microscopy observations in magnetite grains have shown the presence of both the lamellar twins and different monoclinic orientations [14]. In LEEM, the twinned monoclinic phase is observed as parallel bands running perpendicular to the $[001]_m$ directions [17]. The bands correspond to the lamellar monoclinic twins which have a surface rumpling of 0.2°, as confirmed by scanning tunneling microscopy [17].

The same area imaged at room temperature was again observed below the Verwey transition, as shown in Fig. 1(d).

The lamellar bands can be observed in the LEEM image as faint lines running along 45° in the upper part of the image [as shown in the zoomed image in Fig. 1(g)], indicating that in such area the monoclinic c axis is along the cubic [$\bar{1}$00] direction (135°, perpendicular to the bands). However, the lamellar lines are oriented along 135° on the right-hand side of the image, indicating that in that region the monoclinic c axis is along 45°. Thus, two grains with different monoclinic c axis are present in the field of view.

The measured electron reflectivity asymmetry, i.e., the asymmetry in the electron reflectivity measured with the electron beam spin direction along the local magnetization orientation and antiparallel to it, is 2.7% at room temperature. This is not the true asymmetry, as the electron beam polarization in our setup cannot exceed 50% and has been measured to be close to 20%. In consequence, the real reflectivity should be in the range of 13.5%. The experimental asymmetry increases smoothly with decreasing the temperature up to 3% below T_v. We do not detect any significant change when going through either the spin reorientation transition or the Verwey transition. The spin asymmetry of the electron reflectivity reflects in a nontrivial way the magnetic moment of the near-surface region. Thus, the absence of large changes of the electron reflectivity indicates that the magnetic moment does not vary significantly through either transition. Large changes in the magnetic moment through the Verwey transition for a thin film have been reported by polarized neutron reflectometry [38], contrary to previous observations by x-ray magnetic circular dichroism (XMCD) [39]. Our results rule out such large changes for the near-surface region. In support for the same conclusion we have previously reported that the structure of the reconstructed $\sqrt{2} \times \sqrt{2}R45°$ surface does not change through the Verwey transition [17]. However, we are blind to possible changes in the magnetic moment deeper in the crystal.

The magnetic domain distribution has changed completely from the room-temperature one [Fig. 1(e)]. Instead of the wavy bands and curved domain walls, straight domain walls separating large domains with uniform magnetization are observed. Using the same color scheme, the image shows four different domains. In most of the field of view, two domains have the magnetization pointing at 135° (green) and at 315° (purple), respectively. Recalling that in this area the monoclinic c axis is along 135°, it is clear that the surface magnetic easy axis is now along that axis. Likewise, the other two domains, at the right side of the field of view, are oriented along 225° (blue) and along 45° (yellow). Thus, the easy axis is in all cases along the local monoclinic c axis.

In the low-temperature phase, two different types of magnetic domain walls can be distinguished, i.e., 90° and 180° domain walls. In Fig. 1(e) [and the zoom shown in Fig. 1(h)], the walls between the purple and green domains and between the blue and yellow ones separate domains with opposite magnetization, i.e., there are 180° domain walls. They are located in areas with the same overall c axis, being thus pure magnetic domain walls. In contrast, the domain walls between the green and blue and between the purple and yellow domains are 90° magnetic domain walls and coincide with structural domain boundaries. Close inspection of the color-coded magnetization vector images shows that the rotating spin structures within the domain walls are resolved in both types of walls. Within the 180° domain walls, the magnetization is observed to be oriented perpendicular to the magnetization of the adjacent domains. The zoom of Fig. 1(h) shows in detail a section of domain boundary between green (135°) and purple (315°) domains. The boundary appears in blue color (225°) through the upper half of the wall while it is yellow (45°) in the lower part. This indicates a Néel-type spin structure with clockwise (in the blue part) and counterclockwise (in the yellow part) rotation sense. Within the 90° walls, the observed magnetization points in the intermediate direction between the magnetization in the adjacent magnetic domains. For example, it is cyan (180°) for the wall between the green (135°) and blue (225°) domains. The different types of domain walls are consistent with micromagnetic simulations by Kasama and co-workers [compare Fig. 1(e) with Fig. 5 of Ref. [14]].

The magnetic domain wall width at room temperature and at 100 K differ. For the former case, the width can range up to 0.7 μm, but it is highly variable. For the latter, below the Verwey transition, the domain walls have a constant width of 170 ± 40 nm. We do not find a significant difference between the width of the pure magnetic domains and the magnetic domains pinned down between monoclinic domains. To put the width of these domain walls in context, we remark that in all cases we are imaging Néel caps of underlying domain walls: we do not see any out-of-plane component. In the bulk, the Bloch domain walls are thinner, both in cubic and monoclinic magnetite. For magnetite in the cubic phase at RT the walls are typically 100 nm thick [40]. The micromagnetic simulations of Kasama *et al.* [14] show domain walls in the monoclinic phase about 30 nm thick.

Now, we turn to the evolution of the domains in the temperature range from room temperature and below T_v. By observing the onset of the lamellar twin appearance, T_v can be determined in the near-surface region. The observed T_v at the surface for the natural crystal is 112 K (108 K) when heating (cooling). We have also measured a synthetic crystal with good stoichiometry, obtaining a transition temperature of 119 and 118 K. As expected, the better stoichiometry of the synthetic crystal is reflected in a higher T_v. We note, however, that even if the natural crystal is not stoichiometric, it still presents a first-order Verwey transition, as shown by the detection of the lamellar twins. From the decrease of the Verwey temperature [16], the deviation from stoichiometry $Fe_{3(1-\delta)}O_4$ can be estimated to be $\delta \sim 0.005$. In order to determine the evolution of domains through the spin reorientation transition, we have imaged the same area while cooling the sample from 157 to 114 K, switching the electron beam spin-polarization direction every few frames. We have combined, again, the information from images with magnetic contrast along orthogonal directions to provide the magnetization vector maps shown in Fig. 2.

Starting from room temperature, and cooling through 157 and 154 K, no new easy axis directions appear [Figs. 2(a) and 2(b)]. The spread of magnetization angles is larger than at room temperature, effect that we ascribe to thermal drift. However, when cooling down to 144 K [Fig. 2(c)], a new domain structure appears in the upper left side of the field of view, with green and yellow colors corresponding to 45° and 135° magnetization directions. Likewise, in the polar histogram small lobes appear which correspond to domains magnetized along the 45° and 135° orientations. These magnetization

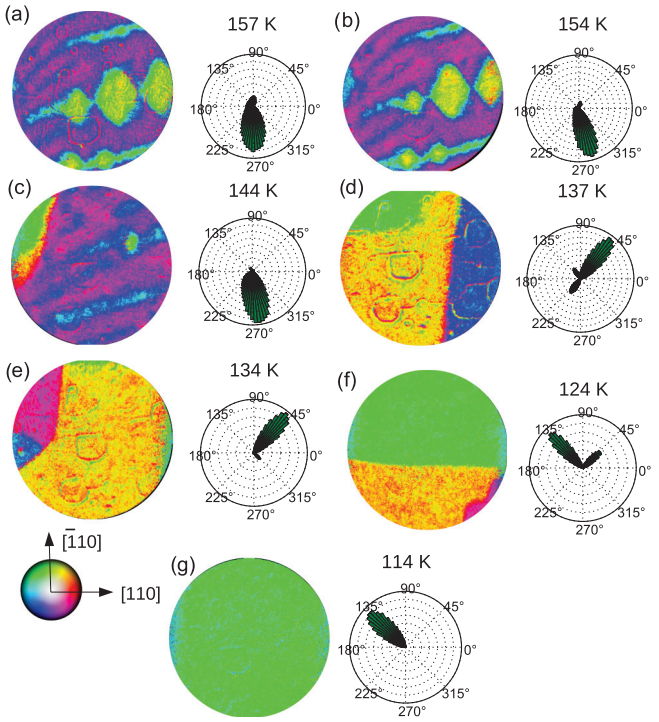

FIG. 2. Evolution of magnetic domains upon cooling from room temperate down to just above the Verwey temperature, through the spin reorientation transition. For each temperature, both the real-space image (left frame) and the polar histogram of the magnetization (right frame) are shown. The field of view of all the images is 12 μm.

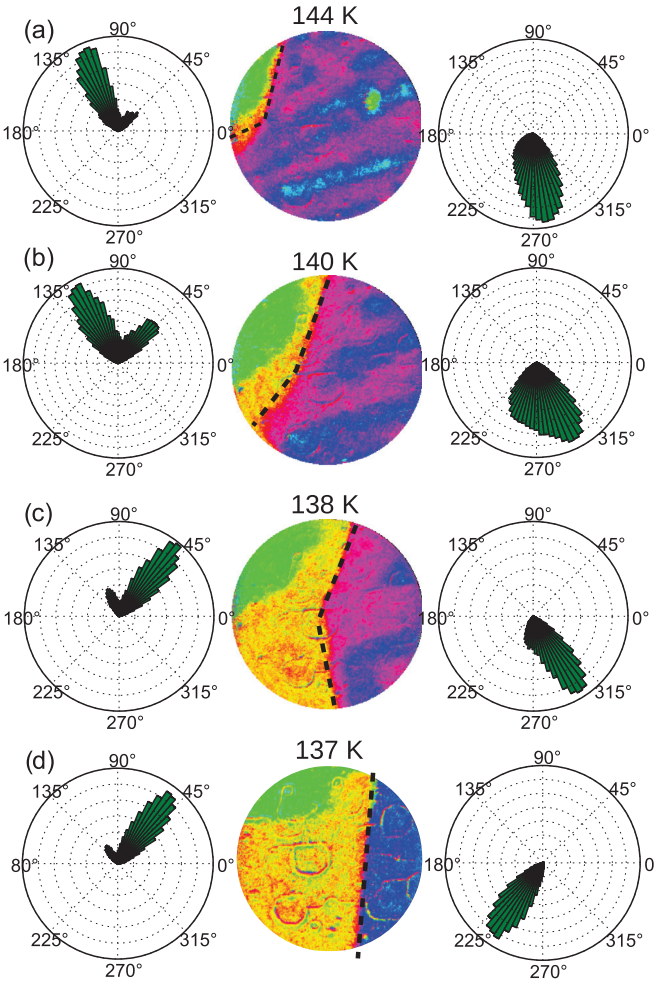

FIG. 3. Detail of the evolution of the magnetic domains through the spin reorientation transition. (a), (b), (c), and (d) correspond, respectively, to 144, 140, 138, and 137 K. For each temperature, the color 2D magnetization image is shown in the center. The dashed lines indicate the boundary used to split the surface area into the regions used in the left- and right-hand-side histograms. The field of view of all the images is 12 μm.

directions were not present before. They correspond to the in-plane ⟨100⟩ directions and thus indicate the start of the spin reorientation transition. By the next frame, at 137 K, all the magnetization vectors are along the in-plane ⟨100⟩ directions, with three large domains (green, yellow, blue) oriented along 135°, 45°, and 225° orientations [Fig. 2(d)]. The domain wall between the first two domains is ragged and it corresponds to a 90° domain wall. The wall between the yellow and blue domains is quite straight, and shows a change of rotation sense: it is green in the upper side while reddish in the lower one. In the range down to the Verwey transition, the domains keep changing, often very rapidly. Still the domain boundaries can be observed. In the frame acquired at 134 K [Fig. 2(e)], the wall between the blue and yellow domains is magenta through the field of view. At the next frame, a single domain sweeps through the area and eventually by 114 K, just above the Verwey transition for this crystal, the full field of view is a single domain covering tens of microns [Fig. 2(g)]. No changes are observed in the topographic images for all the images in Fig. 2.

In Fig. 3, we show the changes of the domains through the spin reorientation transition. The first frame has also been shown in Fig. 2(c). In Fig. 3(a), the distribution of the magnetization is shown separately for the region on the upper-left corner (left histogram) and for the rest of the surface (right histogram). In this way, the larger area of one region does not swamp the magnetization plot measured in the smaller one and, furthermore, we can track the changes in both areas. In the right part of the image, bluish pink mostly, the magnetic easy axes are the same as in the higher-temperature frames: the magnetization points mostly along 270° (downward in plane), which corresponds to the [1$\bar{1}$0] orientation. In contrast, the green area bounded partially by a yellow one has new orientations, along 45° and between 90° and 135°.

In the next frame, the green area has grown to occupy one third of the image, and it shows a wide yellow border, detected also in the corresponding histogram. The remaining area of the image has the magnetization mostly in the direction observed at higher temperatures, but the spread of magnetization angles is much wider (thermal drift was comparable in both frames). By the third frame [138 K, Fig. 3(c)], the green domain has stopped growing, and the yellow ribbon has extended into a large domain itself. But, the mostly pink-blue area on the right now has an average magnetization which is oriented closer to the [100] in-plane orientation (315°). The data suggest that the spin reorientation transition takes place in two stages: first the nucleation of domains with in-plane ⟨100⟩ orientation and their growth gives rise to a discontinuous change of magnetization.

This is followed by a continuous rotation from the ⟨110⟩ to the ⟨100⟩ directions detected in the remaining area under observation. Between the last two frames, while the area on the left side does not change any more, the right-hand side has switched very rapidly from the [100] orientation to the $[0\bar{1}0]$ one.

To consider a possible origin of this two-stage transition, we start from energy considerations [2,41]. In a single-domain crystal with cubic magnetocrystalline anisotropy the evolution of the easy axes upon a change of K_1 depends on the sign of K_2. If K_1 goes from negative values to positive and K_2 remains positive, two consecutive transitions are expected: a discontinuous one between ⟨111⟩ and ⟨110⟩ easy axes, followed by a continuous one from ⟨110⟩ to ⟨100⟩ ones. Instead, if $K_2 < 0$, no intermediate transition to [110] easy axes is expected, and a single discontinuous transition from ⟨111⟩ to ⟨100⟩ should be observed.

So far, the sign of K_2 in magnetite through the spin reorientation transition has not been unequivocally determined. Aragón [6] indicated that it was negative (with a thermal dependence similar to K_1), but remarked that the uncertainties were at least an order of magnitude larger than for K_1. Instead, Belov [13] cites a positive value attributed to Bickford. Thus, if the latter is the case, then two transitions, one discontinuous and another continuous, would be expected. Otherwise, only a single discontinuous transition should be observed. That we observe a two-step transition is in line with a positive value of K_2 through the spin reorientation transition.

We caution, however, that we do not observe the expected orientations for $K_2 > 0$. Instead, we observed the initial nucleation of in-plane ⟨100⟩ surface domains, and then a smooth evolution from in-plane ⟨110⟩ to in-plane ⟨100⟩ ones. Of course, we are not in a single-domain situation, and we have the added complication of the sample geometry, i.e., we are at the surface of an approximately semi-infinite crystal. In this region, even at room temperature, the shape anisotropy dominates the magnetocrystalline one as shown by the observation of in-plane ⟨110⟩ easy axes instead of the bulk ⟨111⟩ expected ones. This influence of the shape anisotropy is more extreme closer to the spin reorientation transition, where with decreasing magnetocrystalline anisotropy the characteristic domain-wall thickness becomes extremely large. Micromagnetic simulations are thus very difficult to apply due to the large scales involved, and even the magnetic domain concept may be of limited applicability too close to the reorientation transition. Thus, further work will be needed to understand the observed two-stage evolution of the magnetic domains in more detail.

IV. SUMMARY

We have observed in real space with nanometer resolution the magnetic domain evolution on a magnetite (001) surface by means of spin-polarized low-energy electron microscopy. The easy axis directions are directly observed to switch in real space from the in-plane ⟨110⟩ directions for room temperature to the in-plane ⟨100⟩ directions below the spin reorientation transition and then to the local monoclinic c axis in the below-Verwey phase. No significant change in the spin-dependent electron reflectivity is detected through either transition, indicating that there is no change in the surface magnetization. Through the spin reorientation transition, a complex multistage process is observed. While initially the growth of new domains oriented along the ⟨100⟩ directions is observed, at a later stage the remaining areas appear to change orientation. Our observations might help into the understanding of the detailed evolution of the magnetocrystalline anisotropy of magnetite. Finally, the study of the evolution of magnetic domains through the spin reorientation transition (and the Verwey transition itself) in magnetite would benefit from the thickness control available in thin films of the type commonly employed for spintronic applications, although we caution that the films must be grown without antiphase domain boundaries which otherwise dominate the magnetic behavior.

ACKNOWLEDGMENTS

We thank Dr. A. T. N'Diaye for his support with the scripts for the color representation of the magnetization. This research was partly supported by the Spanish Ministry of Economy and Competitiveness (MINECO) under Projects No. MAT2011-52477-C5-2-P, No. MAT2012-38045-C04-01, and No. MAT2015-64110-C2-1-P. G.S.P. and R.B. acknowledge funding from the Austrian Science Fund START prize Y 847-N20 and Project No. P24925-N20. Experiments were performed at the Molecular Foundry, Lawrence Berkeley National Laboratory, supported by the Office of Science, Office of Basic Energy Sciences, Scientific User Facilities Division, of the U. S. Department of Energy under Contract No. DE-AC02-05CH11231. L.M.-G. thanks the MINECO for an FPI contract with reference Contract No. BES-2013-063396. R.B. acknowledges a stipend from the TU Wien and Austrian Science Fund doctoral college Solids4Fun (Project No. W1243). A.M. thanks the support of the Spanish Ministry of Education through Project No. PRX14/00307.

[1] R. M. Cornell and U. Schwertmann, *The Iron Oxides* (Wiley, New York, 1997).

[2] A. Hubert and R. Schäfer, *Magnetic Domains: The Analysis of Magnetic Microstructures* (Springer, Berlin, 1998).

[3] E. J. W. Verwey, Electronic conduction of magnetite Fe_3O_4 and its transition point at low temperatures, Nature **144**, 327 (1939).

[4] L. R. Bickford, Jr., Ferromagnetic resonance absorption in magnetite single crystals, Phys. Rev. **78**, 449 (1950).

[5] K. Abe, Y. Miyamoto, and S. Chikazumi, Magnetocrystalline anisotropy of low temperature phase of magnetite, J. Phys. Soc. Jpn. **41**, 1894 (1976).

[6] R. Aragón, Cubic magnetic anisotropy of nonstoichiometric magnetite, Phys. Rev. B **46**, 5334 (1992).

[7] A. R. Muxworthy and E. McClelland, Review of the low-temperature magnetic properties of magnetite from a rock magnetic perspective, Geophys. J. Int. **140**, 101 (2000).

[8] Ö. Özdemir and D. J. Dunlop, Low-temperature properties of a single crystal of magnetite oriented along principal magnetic axes, Earth Planet. Sci. Lett. **165**, 229 (1999).

[9] R. Řezníček, V. Chlan, H. Štěpánková, P. Novák, and M. Maryško, Magnetocrystalline anisotropy of magnetite, J. Phys.: Condens. Matter **24**, 055501 (2012).

[10] M. Bimbi, G. Allodi, R. De Renzi, C. Mazzoli, and H. Berger, Muon spin spectroscopy evidence of a charge density wave in magnetite below the Verwey transition, Phys. Rev. B **77**, 045115 (2008).

[11] P. Novák, H. Štěpánková, J. Englich, J. Kohout, and V. A. M. Brabers, NMR in magnetite below and around the Verwey transition, Phys. Rev. B **61**, 1256 (2000).

[12] Z. Kąkol and J. M. Honig, Influence of deviations from ideal stoichiometry on the anisotropy parameters of magnetite $Fe_{3(1-\delta)}O_4$, Phys. Rev. B **40**, 9090 (1989).

[13] K. P. Belov, Electronic processes in magnetite (or, Enigmas of magnetite), Phys. Usp. **36**, 380 (1993).

[14] T. Kasama, N. S. Church, J. M. Feinberg, R. E. Dunin-Borkowski, and R. J. Harrison, Direct observation of ferrimagnetic/ferroelastic domain interactions in magnetite below the Verwey transition, Earth Planet. Sci. Lett. **297**, 10 (2010).

[15] T. Kasama, R. J. Harrison, N. S. Church, M. Nagao, J. M. Feinberg, and R. E. Dunin-Borkowski, Ferrimagnetic/ferroelastic domain interactions in magnetite below the Verwey transition. part I: electron holography and Lorentz microscopy, Phase Trans. **86**, 67 (2013).

[16] R. Aragón, D. J. Buttrey, J. P. Shepherd, and J. M. Honig, Influence of nonstoichiometry on the Verwey transition, Phys. Rev. B **31**, 430 (1985).

[17] J. de la Figuera, Z. Novotny, M. Setvin, T. Liu, Z. Mao, G. Chen, A. T. N'Diaye, M. Schmid, U. Diebold, A. K. Schmid, and G. S. Parkinson, Real-space imaging of the Verwey transition at the (100) surface of magnetite, Phys. Rev. B **88**, 161410 (2013).

[18] J. de la Figuera, L. Vergara, A. T. N'Diaye, A. Quesada, and A. K. Schmid, Micromagnetism in (001) magnetite by spin-polarized low-energy electron microscopy, Ultramicroscopy **130**, 77 (2013).

[19] N. Rougemaille and A. K. Schmid, Magnetic imaging with spin-polarized low-energy electron microscopy, Eur. Phys. J. Appl. Phys. **50**, 20101 (2010).

[20] K. Grzelakowski, T. Duden, E. Bauer, H. Poppa, and S. Chiang, A new surface microscope for magnetic imaging, IEEE Trans. Magn. **30**, 4500 (1994).

[21] T. Duden and E. Bauer, A compact electron-spin-polarization manipulator, Rev. Sci. Instrum. **66**, 2861 (1995).

[22] R. Ramchal, A. K. Schmid, M. Farle, and H. Poppa, Spiral-like continuous spin-reorientation transition of Fe/Ni bilayers on Cu(100), Phys. Rev. B **69**, 214401 (2004).

[23] F. El Gabaly, S. Gallego, C. Muñoz, L. Szunyogh, P. Weinberger, C. Klein, A. K. Schmid, K. F. McCarty, and J. de la Figuera, Imaging Spin-Reorientation Transitions in Consecutive Atomic Co Layers on Ru(0001), Phys. Rev. Lett. **96**, 147202 (2006).

[24] F. El Gabaly, K. F McCarty, A. K Schmid, J. de la Figuera, M. C. Muñoz, L. Szunyogh, P. Weinberger, and S. Gallego, Noble metal capping effects on the spin-reorientation transitions of Co/Ru(0001), New J. Phys. **10**, 073024 (2008).

[25] Surface Preparation Laboratory, www.spl.eu

[26] F. Walz, The Verwey transition-a topical review, J. Phys.: Condens. Matter **14**, R285 (2002).

[27] G. S. Parkinson, Iron Oxide Surfaces, Surf. Sci. Rep. (2016), doi:10.1016/j.surfrep.2016.02.001 [arXiv:1602.06774].

[28] S. Nie, E. Starodub, M. Monti, D. A. Siegel, L. Vergara, F. El Gabaly, N. C. Bartelt, J. de la Figuera, and K. F. McCarty, Insight into magnetite's redox catalysis from observing surface morphology during oxidation, J. Am. Chem. Soc. **135**, 10091 (2013).

[29] R. Bliem, E. McDermott, P. Ferstl, M. Setvin, O. Gamba, J. Pavelec, M. A. Schneider, M. Schmid, U. Diebold, P. Blaha, L. Hammer, and G. S. Parkinson, Subsurface cation vacancy stabilization of the magnetite (001) surface, Science **346**, 1215 (2014).

[30] L. Martín-García, R. Gargallo-Caballero, M. Monti, M. Foerster, J. F. Marco, L. Aballe, and J. de la Figuera, Spin and orbital magnetic moment of reconstructed $\sqrt{2} \times \sqrt{2}$R45° magnetite(001), Phys. Rev. B **91**, 020408 (2015).

[31] E. Bauer, Spin-polarized low energy electron microscopy, in *Modern Techniques for Characterizing Magnetic Materials*, edited by Yimei Zhu (Springer, New York, 2005), pp. 361.

[32] Y. Z. Chen, J. R. Sun, Y. N. Han, X. Y. Xie, J. Shen, C. B. Rong, S. L. He, and B. G. Shen, Microstructure and magnetic properties of strained Fe_3O_4 films, J. Appl. Phys. **103**, 07D703 (2008).

[33] A. D. Wei, J. R. Sun, Y. Z. Chen, W. M. Lü, and B. G. Shen, The influence of film thickness on photovoltaic effect for the $Fe_3O_4/SrTiO_3$:Nb heterojunctions, J. Phys. D: Appl. Phys. **43**, 205004 (2010).

[34] A. Hamie, Y. Dumont, E. Popova, A. Fouchet, B. Warot-Fonrose, C. Gatel, E. Chikoidze, J. Scola, B. Berini, and N. Keller, Investigation of high quality magnetite thin films grown on $SrTiO_3$(001) substrates by pulsed laser deposition, Thin Solid Films **525**, 115 (2012).

[35] M. Monti, M. Sanz, M. Oujja, E. Rebollar, M. Castillejo, F. J. Pedrosa, A. Bollero, J. Camarero, J. L. F. Cuñado, N. M. Nemes, F. J. Mompean, M. Garcia-Hernández, S. Nie, K. F. McCarty, A. T. N'Diaye, G. Chen, A. K. Schmid, J. F. Marco, and J. de la Figuera, Room temperature in-plane ⟨100⟩ magnetic easy axis for $Fe_3O_4/SrTiO_3$(001):Nb grown by infrared pulsed laser deposition, J. Appl. Phys. **114**, 223902 (2013).

[36] D. T. Margulies, F. T. Parker, M. L. Rudee, F. E. Spada, J. N. Chapman, P. R. Aitchison, and A. E. Berkowitz, Origin of the Anomalous Magnetic Behavior in Single Crystal Fe_3O_4 Films, Phys. Rev. Lett. **79**, 5162 (1997).

[37] E. K. H. Salje, Ferroelastic materials, Annu. Rev. Mater. Res. **42**, 265 (2012).

[38] M. B. Yazdi, M. Major, A. Wildes, F. Wilhelm, A. Rogalev, W. Donner, and L. Alff, Possible evidence for a spin-state crossover in the Verwey state in Fe_3O_4 thin films, Phys. Rev. B **93**, 014439 (2016).

[39] E. J. Goering, M. Lafkioti, S. Gold, and G. Schuetz, Absorption spectroscopy and XMCD at the Verwey transition of Fe_3O_4, J. Magn. Magn. Mater. **310**, e249 (2007).

[40] W. Williams and T. M. Wright, High-resolution micromagnetic models of fine grains of magnetite, J. Geophys. Res. **103**, 30537 (1998).

[41] K. P. Belov, A. K. Zvezdin, A. M. Kadomtseva, and R. Z. Levitin, Spin-reorientation transitions in rare-earth magnets, Sov. Phys.–Usp. **19**, 574 (1976).